Technical aspects of osteoid osteoma ablation in children using MR-guided high intensity focussed ultrasound

Pavel S. Yarmolenko, Avinash Eranki, Ari Partanen, Haydar Celik, AeRang Kim, Matthew Oetgen, Viktoriya Beskin, Domiciano Santos, Janish Patel, Peter C. W. Kim & Karun Sharma

Taylor & Francis
Taylor & Francis Group

Check for updates

Technical aspects of osteoid osteoma ablation in children using MR-guided high intensity focussed ultrasound

Pavel S. Yarmolenko[a], Avinash Eranki[a], Ari Partanen[b], Haydar Celik[a], AeRang Kim[c], Matthew Oetgen[d], Viktoriya Beskin[e], Domiciano Santos[f], Janish Patel[f], Peter C. W. Kim[a] and Karun Sharma[a,e]

[a]Sheikh Zayed Institute for Pediatric Surgical Innovation, Children's National Medical Center, Washington, DC, USA; [b]Clinical Science MR Therapy, Philips, Andover, MA, USA; [c]Oncology, Children's National Medical Center, Washington, DC, USA; [d]Orthopedics, Children's National Medical Center, Washington, DC, USA; [e]Radiology, Children's National Medical Center, Washington, DC, USA; [f]Anesthesiology, Children's National Medical Center, Washington, DC, USA

ABSTRACT

Background: Osteoid osteoma (OO) is a painful bone tumour occurring in children and young adults. Magnetic resonance imaging-guided high intensity focussed ultrasound (MR-HIFU) allows non-invasive treatment without ionising radiation exposure, in contrast to the current standard of care treatment with radiofrequency ablation (RFA). This report describes technical aspects of MR-HIFU ablation in the first 8 paediatric OO patients treated in a safety and feasibility clinical trial (total enrolment of up to 12 patients).

Materials and methods: OO lesions and adjacent periosteum were treated with MR-HIFU ablation in 5–20 sonications (sonication duration $= 16$–48 s, frequency $= 1.2$ MHz, acoustic power $= 20$–160 W). Detailed treatment workflow, patient positioning and coupling strategies, as well as temperature and tissue perfusion changes were summarised and correlated.

Results: MR-HIFU ablation was feasible in all eight cases. Ultrasound standoff pads were shaped to conform to extremity contours providing acoustic coupling and aided patient positioning. The energy delivered was 10 ± 7 kJ per treatment, raising maximum temperature to $83 \pm 3\,°C$. Post ablation contrast-enhanced MRI showed ablated volumes ranging 0.46–19.4 cm^3 extending further into bone (7 ± 4 mm) than into soft tissue (4 ± 6 mm, $p = 0.01$, Mann–Whitney). Treatment time ranged 30–86 min for sonication and 160 ± 40 min for anaesthesia. No serious treatment-related adverse events were observed. Complete pain relief with no medication occurred in 7/8 patients within 28 days following treatment.

Conclusions: MR-HIFU ablation of painful OO appears technically feasible in children and it may become a non-invasive and radiation-free alternative for painful OO. Therapy success, efficiency, and applicability may be improved through specialised equipment designed more specifically for extremity bone ablation.

Introduction

Osteoid osteoma (OO) is a benign, but painful bone lesion that usually affects children and young adults between 10 and 20 years of age [1]. The most frequent symptom is localised bone pain that worsens at night and is alleviated by nonsteroidal anti-inflammatory drugs (NSAIDs) [2]. The pain results from prostaglandin release by the OO nidus – a highly vascularised central region often surrounded by a fibrovascular rim and reactive sclerosis [3]. Complete and permanent pain resolution can be achieved through destruction of the OO nidus and adjacent periosteal nerves [1].

Difficulty in intraoperative localisation of the OO nidus makes open surgical resection challenging and involves significant bone resection and collateral damage [1]. To address the long hospital stays and recovery times associated with open surgical resection, CT-guided radiofrequency ablation (RFA) has become the standard of care treatment for OO refractory to medical management over the course of the last two decades [4,5]. While RFA has very high clinical success rates, it is an invasive procedure, which requires drilling from the skin through soft tissue and bone to burn the OO nidus with a probe. Image guidance with CT also exposes the patient and the physician to ionising radiation.

Magnetic resonance imaging (MRI)-guided high intensity focussed ultrasound (MR-HIFU) may address the inadequacies of open surgery and RFA by providing a completely non-invasive and spatially precise ablation of tissue without ionising radiation. This therapeutic modality uses detailed anatomical MRI for treatment planning and multi-slice MRI thermometry for real-time therapy monitoring and control.

Various benign and malignant lesions have been treated with MR-HIFU, including uterine fibroids as well as prostate, brain and musculoskeletal tumours [6]. Safety, feasibility, and effectiveness of MR-HIFU ablation of metastatic bone lesions and periosteal nerves to alleviate pain has also been shown [7]. More recently, MR-HIFU was used by Napoli et al. to treat 29 patients (mean age $= 25 \pm 16$) with painful OO, achieving >90% treatment success with no major treatment-associated adverse events [8,9]. Their initial study showed that MR-HIFU ablation of OO was feasible and safe using the InSightec ExAblate MR-HIFU system. Detailed information on procedure workflow, patient positioning, imaging and sonication parameters would help guide and develop this application of MR-HIFU.

This work focuses on the technical aspects of eight MR-HIFU OO ablation treatments performed at our institution through an IRB-approved clinical trial designed to evaluate the safety and feasibility of this therapy in a paediatric cohort, in whom OO is most commonly seen. Our study complements previously published work [8,9] by examining a younger patient population and using a different clinical MR-HIFU device. This interim report specifically addresses procedure workflow, patient positioning and acoustic coupling strategies, MR imaging and sonication parameters using the Philips Sonalleve V2 clinical MR-HIFU system. We also discuss therapy duration, target temperature achieved, thermal dose and non-perfused volume (NPV) resulting from the treatment.

Materials and methods

Patients

Eight patients with radiologically confirmed diagnosis of OO were treated on a prospective clinical trial of MR-HIFU ablation of OO in children and young adults, with a total planned enrolment of up to 12 patients (NCT02349971, [10]). All patients enrolled in this trial received treatment after providing a written informed consent, and all procedures were approved by the Children's National Health System institutional review board.

MR imaging

A clinical MRI scanner (Achieva 1.5 T, Philips, Best, the Netherlands) was used in conjunction with other MR-HIFU system components for pre-treatment imaging, real-time guidance, and post-treatment assessment (Table 1), as briefly summarised below.

Following generic survey and reference scans, a high-resolution 3D dataset was examined to ensure that no air bubbles were present on the patient's skin in the likely HIFU beam path. For treatment planning, both T1- and T2-weighted 3D datasets were acquired to ensure sufficient contrast and visibility of the small OO nidus, neurovascular bundles and other surrounding anatomy.

Real-time MRI thermometry was performed using the proton resonance frequency shift (PRFS) method [11]. A near-field imaging slice was positioned in the plane that is approximately perpendicular to the HIFU beam, capturing either muscle adjacent to the fat or gel pad next to the skin if muscle thickness was insufficient (<7 mm).

Post-treatment MR imaging began 3 min after the last sonication ended to limit the effect of heat on tissue T1 and T2 values. The same T1- and T2-weighted scans were repeated after therapy and followed by manual infusion (1–2 ml/s) of MRI contrast agent (Dotarem®, 0.1 mmol/kg (0.2 ml/kg), Guerbet LLC, Bloomington, IN) and 5 ml saline flush. The T1-weighted scan was then repeated again.

MR-HIFU treatment

A clinical MR-HIFU system (Sonalleve V2, Philips, Vantaa, Finland) was used to thermally ablate the OO nidus and adjacent periosteal nerves, as summarised briefly below and in Figure 1. Six of the eight treated patients were positioned on the HIFU tabletop prior to induction of anaesthesia to acquire initial images used to pre-plan the treatment and to select a comfortable patient and target limb position with the aid of patient feedback and appropriate cushioning. Following onset of general anaesthesia, the patients were positioned on the MR-HIFU table. Planning image sets were acquired, followed by OO ablation and post-treatment contrast enhanced imaging. Further details on the equipment and details of the procedure are provided in "Supplemental Materials and Methods".

Technical feasibility assessment

Technical feasibility was assessed using pre-treatment imaging and confirmed when appropriate patient positioning and ablation were completed on treatment day. Treatment was considered "feasible" if the patient was successfully positioned in a way that allowed for treatment without

Table 1. Overview of MRI sequences used for MR-HIFU treatment of OO. Field of view (FOV) for the real-time MR thermometry sequence was standardised at 400 × 400 mm, with three orthogonal slices intersecting at the current focus and one slice manually placed to monitor near field temperature. For all other scans, FOV and number of slices were minimised to conform to anatomy and minimise acquisition time.

| MRI sequences and their purpose	Type	TR (ms)	TE (ms)	FA (°)	NSA	Voxel size (mm)	Slices	Duration (min:s)
Survey – target localisation	2D TFE	11.0	6.9	25	2	0.74 × 0.74 × 10	16	1:27
Reference – coil calibration	Reference							1:08
Air bubble detection – skin protection	3D FFE	15.0	12.0	10	2	1.1 × 1.1 × 2.0	Varied	< 4 min
T2w – treatment planning and evaluation	3D TSE	1400	186	90	2	1.3 × 1.3 × 2.6	Varied	< 4 min
T1w scans – therapy planning and evaluation (pre- and post-treatment and post-contrast)	3D FFE	6.4	3.1	10	2	1.3 × 1.3 × 2.6	Varied	1:55–6:30
MR thermometry – treatment monitoring and control	2D FFE	54	30	19	1	2.5 × 2.5 × 7.0	4	0:3.7 dynamic
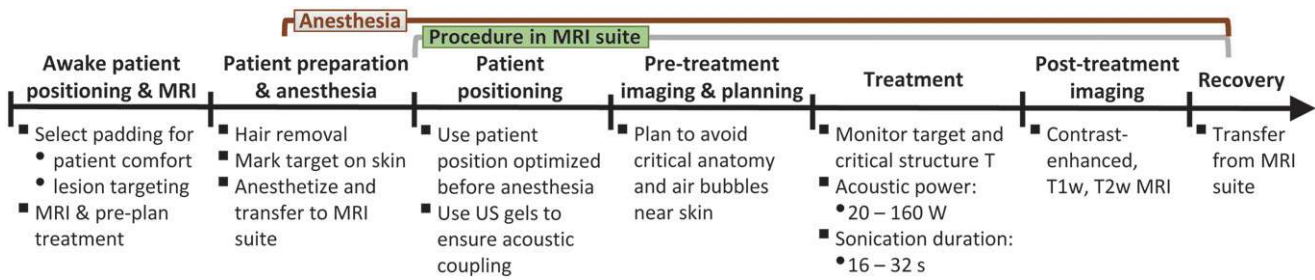
Figure 1. Overview of treatment workflow for osteoid osteoma ablation with MR-HIFU.

Table 2. Summary of patient and lesion characteristics. Reported periosteal thickness and nidus dimensions were calculated from CT images prior to treatment, with no significant differences compared to MRI ($p > 0.57$, t test).

	Mean $\pm$ SD (median, range)
Patients:	
Age (years)	15.8 $\pm$ 5.9 (16.5, 7–24)
Sex (number of males/females)	6/2
Weight (kg)	57 $\pm$ 20 (65.2, 25.2–75.2)
Height (cm)	161 $\pm$ 19 (167.5, 120–177)
BMI	21 $\pm$ 4 (21.2, 14.4–27.3)
Lesions:	
Skin-to-bone distance at target lesion (mm)	32 $\pm$ 16 (31.9, 16–60)
Periosteal thickness at target lesion (mm)	4 $\pm$ 5 (2.5, 0–14)
OO nidus volume (mm^3)	1.0 $\pm$ 0.6 (0.82, 0.4–2.5)
Lesion location	Femur: 3; Tibia: 3; Phalanx: 1; Talus: 1

potentially exposing critical structures, such as nerves, to lethal thermal doses.

Image analysis

Philips Sonalleve Therapy Planning Software (R3.2, Philips, Vantaa, Finland) was used to record power, energy and duration of sonication, maximum temperature and cumulative thermal dose values, as well as to analyse the spatial extent of lethal thermal dose and vascular stasis. NPV was calculated as a volume of a spheroid on subtraction images of the contrast-enhanced T1-weighted scans, using its dimensions in three orthogonal planes. Extent of this volume from the bone surface into the soft tissue and into bone was measured. Periosteal thickness (maximum thickness of the periosteum/bone around the OO nidus) and nidus dimensions in three orthogonal planes were determined on CT imaging using the OsiriX software package (Pixmeo, Geneva, Switzerland).

Statistical analysis

Non-parametric statistical tests were used throughout data analysis. NPV values inside vs. outside of bone were compared using the Mann–Whitney test. Correlations among parameters were analysed using the Spearman correlation statistic. Results were reported as mean $\pm$ SD alongside the median and range of measurements for $n = 8$, unless otherwise specified. Two-tailed p values were obtained and $p \leq 0.05$ was considered significant.

Results

Patient and lesion characteristics

Patient demographics and disease location are described in Table 2. Six of the eight treated patients were below 18 years of age, and two were in their early twenties. All but one of the patients was 145–170 cm tall. There was a large range of lesion depths and periosteum thickness.

Technical feasibility

Patient positioning on the HIFU table and subsequent treatment were feasible in all 8 cases, with OO locations in the tibia ($n = 3$), femur ($n = 3$), talus ($n = 1$) and phalanx ($n = 1$). Below, we describe patient support and ultrasound coupling strategies, and provide technical details that characterise technical feasibility of OO ablation with MR-HIFU.

Patient positioning

Patients required variable amounts of padding and support due to differences in patient weight and height. Upper-body support for taller patients required extension of the MR-HIFU table by as much as 50 cm (Figure 2), which was accomplished with a combination of hard and soft foam padding. Pre-treatment positioning of six of the eight patients while awake was useful in identifying several patient-table contact points (especially around the edge of the HIFU tabletop acoustic window) that became uncomfortable or painful without extra padding. Patient feedback revealed that softer foam padding was necessary between the patient's body and the top pelvic MR imaging coil that was tightened against the patient's body with Velcro straps. Despite the preparatory positioning prior to anaesthesia, three of the patients exhibited mild discomfort and pain at contact points of their body with the edge of the HIFU window (outside of the treatment area) with scarce padding. The discomfort resolved without treatment over the course of the first week following therapy.

Ultrasound coupling

Gel pads in combination with diluted diagnostic ultrasound gel successfully provided acoustic coupling. Lethal thermal doses were not detected in the vicinity of the skin. Two of the cases required a carved gel pad to better conform to the limb and to support it, providing enough gel-skin contact area to fit the HIFU beam and avoid reflection and off-target

Figure 2. Patient positioning and ultrasound coupling for extremity osteoid osteoma treatments. Patient positioning was feasible in all eight patients. (A,B) extension of the HIFU table was necessary to support the upper body during lower extremity treatment. (C,D) pre-treatment positioning helped identify pressure spots, enabled pre-planning of sonications, and provided guidance for patient positioning. Yellow padding 4 cm in thickness (C&D, hollow blue arrows) was used in place of gel in pre-anaesthesia patient positioning. (E,F) ultrasound coupling gel pads were cut, carved and sometimes combined to ensure HIFU coupling free of air-water interfaces. Note that the outline of the HIFU beam passes directly into the limb while avoiding air through either (E) conformably carved gel pad, or (F) wedge-shaped gel pads (solid red arrows) placed on both sides of the limb, with 1:2 ultrasound gel:water dilution creating continuous coupling (hollow red/white arrows).

heating associated with air interfaces. The need for such modifications was most apparent in areas where the axial limb cross-section was small relative to the HIFU beam (Figure 2(E)).

Duration of the procedure and its components

Pre-treatment patient positioning and imaging was performed prior to anaesthesia for six of the eight treated patients, lasting 20–40 min. Such pre-treatment positioning and imaging was deemed unnecessary for the remaining two patients whose lesions were similar in appearance and location to previously completed treatments. Duration of anaesthetised patient positioning hovered around its average of 28 ± 14 min for most patients, though for the first patient it was prolonged by the need to re-cut the stand-off pad to better fit the anatomy and the need to re-position the patient due to the presence of air bubbles (Figure 3(B)).

For all patients, treatment planning began immediately after the first planning image set was acquired and sent to the HIFU Therapy Planning Console (<8 min into acquisition of pre-treatment MRI). Time spent on acquiring planning image datasets and planning the treatment varied by as much as 30 min (Figure 3(A)) due to the difference in size of the targeted periosteum, proximity to critical structures and other factors, such as operator experience. Required MRI suite time decreased, as did the various components of the procedure, especially after the first patient due to growing experience (Supplemental Figure 1(A,B) and Figure 3). Total MRI suite time averaged 140 ± 30 min. Total anaesthesia time was, on average, 20 min longer (160 ± 40 min), as it included patient transfer to and from the MRI suite, intubation and extubation.

A cooling period followed each sonication, and while duration of individual sonications ranged 16–36 s, the cooling
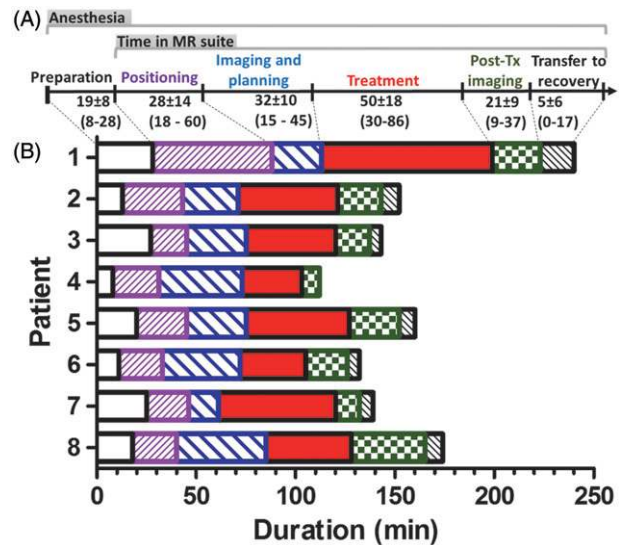

Figure 3. Duration of treatment and its individual components. (A) Treatment workflow with average duration of each workflow component. (B) Relative lengths of all treatment sub-components. "Preparation" included pre-treatment induction of anaesthesia and/or sedation, cleaning and hair removal from the skin at the treatment site as well as pre-treatment transport of the patient into the MRI suite. The duration of "Transfer to recovery" was set to 0 for patient 4, as this patient was not intubated.

period was >3 min for most sonications. Including cool-down times, the 5–20 sonications took 30–86 min, though only 3.4 ± 1.4 min of this time was spent on sonications ("Effective sonication time", Table 3) across all treatments. The rest of the treatment time was used for cooling between sonications and planning subsequent target locations. Treatment duration closely tracked and significantly correlated with the number of sonications (Spearman $r = 0.79$, $p = 0.0279$, Supplemental Figure 1(B)), meaning that the use of fewer, higher power sonications generally decreased treatment time.

Table 3. Summary of sonication duration and power, as well as resulting temperature and tissue perfusion changes.

	Mean ± SD (median, range)
Duration	
Number of therapy sonications	11 ± 4 (11, 5–20)
Effective sonication time (min)	3.4 ± 1.4 (3.2, 1.6–5.7)
Duration of one sonication (s)	18 ± 5 (16, 16–36)
Duration of one sonication + cooling (min)	4.1 ± 0.5 (3.9, 3.5–4.7)
Total treatment duration (min)	49 ± 18 (47.5, 30–86)
Power and energy	
Sonication power (W)	50 ± 30 (50, 15–160)
Total therapy energy (kJ)	10 ± 7 (9.48, 2.1–24.1)
Energy/sonication (J)	970 ± 700 (800, 240–3200)
Temperature and ablation	
Maximum temperature (°C)	83 ± 3 (83.7, 77–87)
Volume of lethal thermal dose (cm³)[a]	1.4 ± 1.1 (1.23, 0.18–3.85)
NPV volume (cm³)[a]	5 ± 6 (2.2, 0.46–19.4)
NPV extent into soft tissue (mm)	5 ± 6 (3.1, 1.0–19.1)
NPV extent into bone (mm)	9 ± 3 (6.9, 5.5–14.9)

[a]Volume of lethal thermal dose was defined separately at each target location, whereas sonications at several target locations contributed to the total NPV volume.

For most patients, the most time-consuming single component of the procedure was sonications (Figure 3). However, all preparatory procedures taken together (Preparation, Positioning, Imaging and Planning) were comparable in duration to the 30–86 min spent on the treatment itself.

Thermometry, energy, and spatial definition of target

The depth of the targeted OO nidus centre from skin surface ranged 1.1–7.7 cm and all lesions were targetable. Thick neocortex was encountered in two cases: one in femur and one in tibia (up to ~12 mm thickening), requiring a higher number of sonications of greater power and duration. Sonications resulted in highest temperatures and near-instantaneous ablation (>60 °C) at the bone surface, with lethal thermal dose delivered to the adjacent soft tissue as well as bone, according to MR thermometry measurements (Figures 4 and 5). Using NPV as an indicator of the extent of the ablated zone, the ablated region extended more into the bone than into soft tissue ($p = 0.01$, Mann–Whitney). No significant correlation was found (Spearman $r = -0.43$, $p = 0.35$) between extent of ablation into the bone and its extent into adjacent soft tissue.

Estimated NPV was $5 \pm 6 \, cm^3$, which was several fold greater than the $1.4 \pm 1.1 \, cm^3$ estimates of a volume treated with a lethal thermal dose at one target location (Table 3). This discrepancy between NPV and lethal thermal dose volume is at least in part due to NPV incorporating the effects of 5–20 therapy sonications at 2–6 locations, whereas thermal dose was estimated at each location separately.

Acoustic power averaged $50 \pm 30 \, W$ and total energy deposition, including all therapeutic sonications, averaged $10 \pm 7 \, kJ$ across all eight patients, ranging 2.1–24.1 kJ (Table 3). Energy prescribed in individual therapeutic sonications varied widely as well, ranging 240–3200 J. Total treatment energy correlated significantly with the resulting NPV volume (Spearman $r = 0.952$, $p = 0.001$). Energy used at each location did not correlate with the volume that achieved lethal thermal dose based on MRI thermometry (Spearman $r = 0.260$, $p = 0.22$).

Near field heating/cooling

Delineation of potentially vulnerable areas prior to treatment allowed close monitoring of their temperature and thermal dose during treatment in all imaged planes. However, some of the targeted lesions had little tissue other than subcutaneous fat between the targeted lesion and the gel pad, making PRFS-based MRI thermometry impossible or difficult between the gel pad and the target. If insufficient thickness of muscle precluded real-time temperature mapping in the near field, then sufficient MRI thermometry was performed using a slice in the gel pad that was parallel and adjacent to the skin in the HIFU beam path (Figure 6(A)).

Several patients had neurovascular tissue that needed to be spared near the target (Figure 6(B)). In such cases, MRI thermometry was performed on a slice in close proximity to the vulnerable structure, between the bone and the vulnerable structure. For one of the patients, near field MRI thermometry was performed 2.5 mm from the heated bone surface. This location was chosen in favour of placing the near field slice in the gel due to the signal being sufficient for MRI thermometry and due to the very shallow location of the OO nidus relative to the bone surface. At this location, the maximum cumulative thermal dose reached 300 CEM43 adjacent to the targeted region (Figure 4, Patient 4 and Figure 6(C,D)). This thermal dose would be lethal in affected tissues [12]. However, this thermal dose was recorded in only a few voxels of the near field monitoring slice. Furthermore, the imaging slices through the centre of the HIFU beam indicated that these elevations in temperature were localised and would not affect the skin (Figure 4, Patient 3, third column), and, therefore, the procedure was completed despite the relatively high-thermal dose in near field monitoring slice. As a result, no skin damage was observed. In all remaining patients, maximum temperature in the near field monitoring slices remained <50 °C, resulting in sub-lethal thermal doses (<10.5 CEM43), known to have only mild functional effects on tissue, if any [12].

Treatment and imaging findings

All patients were monitored for up to four hours after recovery from anaesthesia/sedation, returning to their daily activities the following day. Close follow-up over four weeks after treatment showed that these treatments caused no reportable treatment-related adverse events. For seven of the eight patients, complete or nearly complete resolution of OO-related pain followed within days and all but one patient were able to cease medication use 28 d following treatment.

Although temperature changes within the nidus could not be visualised during the sonications due to relatively low signal there, contrast-enhanced MRI performed immediately after ablation showed complete lack of enhancement (i.e. perfusion) of the OO nidus in six of eight patients, and partial nidus enhancement in two patients. In addition, these scans showed that NPV extended 1.3- to 12-fold deeper into bone
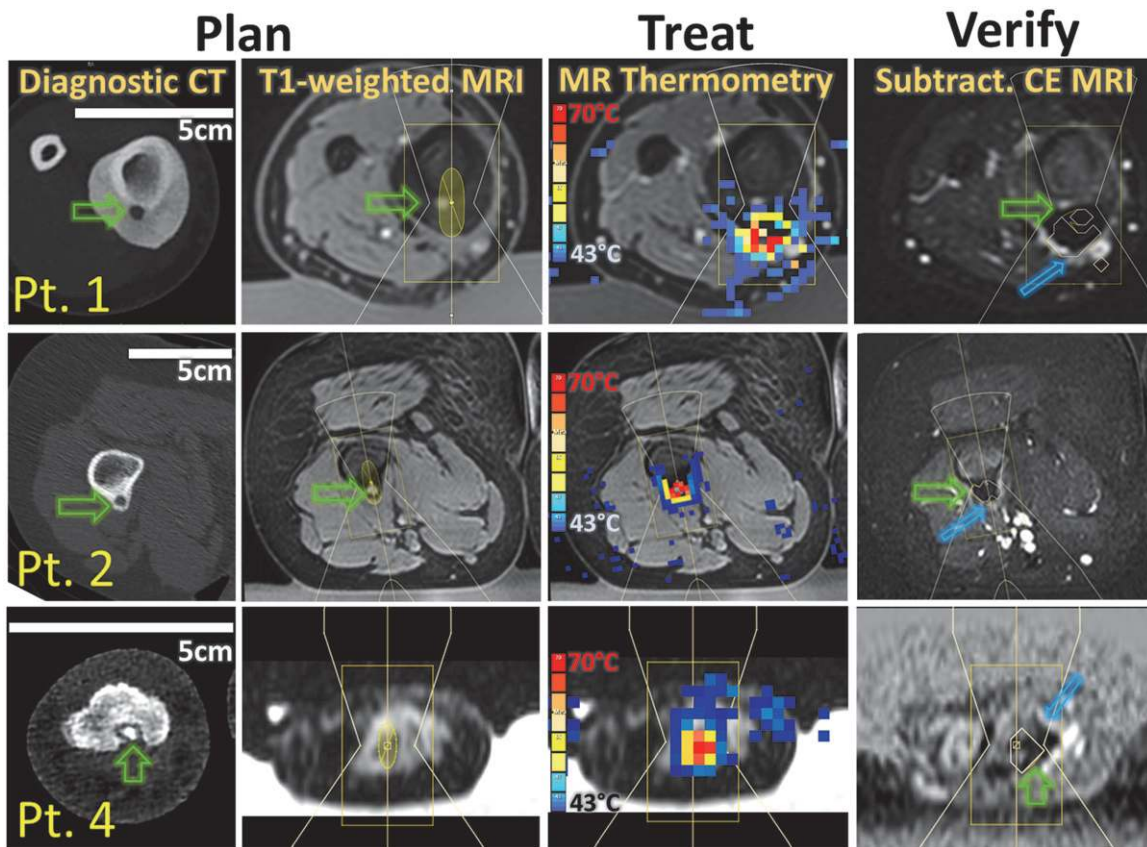
Figure 4. MR-HIFU ablation of osteoid osteoma: from diagnosis to post-treatment imaging. Patients 1, 2 and 4 had lesions in the tibia, the femur, and the phalanx, respectively. *Columns 1 and 2:* Pre-procedure planning was performed using available diagnostic CT and MRI imaging. Note that the length of the 5-cm scale bar differs among patients, highlighting the size difference between the targeted limbs. Green arrows indicate the location of OO nidus. Pre-treatment T1-weighted high-resolution MRI dataset was used to plan treatment. *Column 3:* MRI thermometry allowed for monitoring of heating during treatment (temperature at the end of sonication is shown). *Column 4:* Resulting lack of perfusion was evaluated using a subtraction image of MRI contrast enhancement. Blue arrows mark oedema immediately after treatment and a contour surrounds areas of lethal thermal dose.

than into soft tissue (9 ± 3 mm in bone vs. 5 ± 6 mm in soft tissue, $p = 0.01$, Mann–Whitney).

Discussion

To highlight specific technical aspects relevant to MR-HIFU OO ablation in a young patient cohort, the following discussion compares and contrasts our experience to other recently published work. Among the most relevant, are the published experiences with MR-HIFU of OO in older patients using a different commercial clinical system and MR-HIFU ablation of painful bone metastatic cancer and larger soft tissue tumours.

Technical feasibility

All eight MR-HIFU ablation procedures were technically feasible with regard to successful patient positioning and coupling, treatment planning, sonication under real-time MRI monitoring and post-treatment visualisation of the ablated target. Technical feasibility and treatment safety are both largely dependent on device design, treatment workflow and patient/lesion characteristics. In the case of OO, the bone lesions are relatively small and they are most commonly

located in the extremities. This aspect required positioning aides and patient-specific positioning strategies to enable therapy for all eight patients. In the eight OO cases, a small number of sonications was sufficient to achieve lethal thermal dose around the periphery of the bone and cessation of perfusion in the neocortex surrounding the OO nidus and the nidus itself. While the tabletop-integrated MR-HIFU design may be further tailored for OO treatment, its current design is capable of safely ablating OO.

Design of MR-HIFU: tabletop

In terms of geometric accessibility, the treated lesions were reached with either the focal point or the broad portion of the MR-HIFU beam as planned, and in this respect, tabletop and transducer positioning system provided sufficient lesion access. There is room for clinical MR-HIFU equipment optimisation to accommodate ablation of bony lesions, especially in extremities. This device was originally designed for uterine fibroid ablation in adult patients positioned in prone position. For those patients, a large acoustic window at the centre of the HIFU table allowed for ideal patient position to centre the mid abdomen on the treatment window. The range of transducer motion was sufficient to target relatively
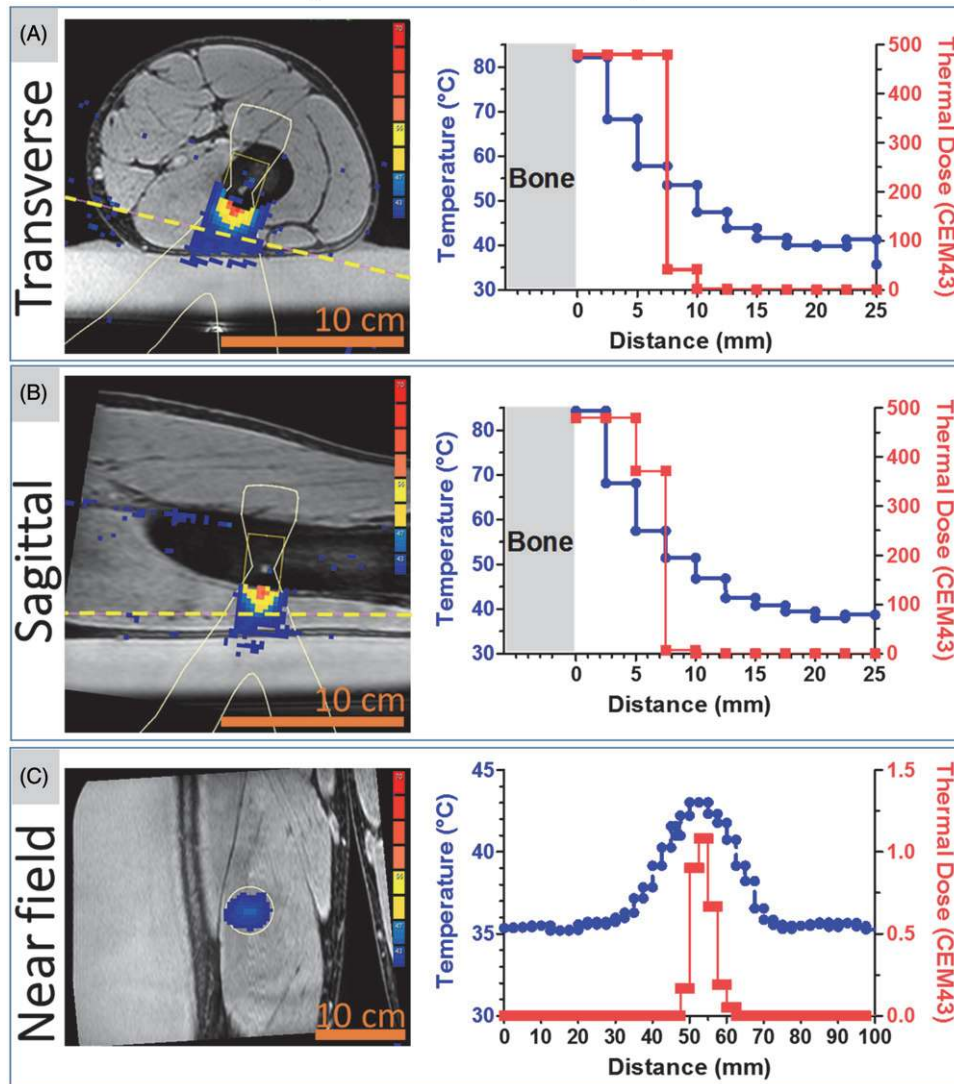
Figure 5. Heat distribution in muscle adjacent to neocortex at the end of sonication. The 4 mm target was sonicated at the maximum acoustic power (160 W) available under our protocol for this cell size, producing 2560 J in 16 s. Panels A, B and C represent the three slices monitored with real-time MRI thermometry (blue-to-red colour map), overlaid on corresponding magnitude images (greyscale) from a T1w planning scan with fat saturation. The near field slice (C) was positioned in the muscle, $\sim$1.5 cm from the bone surface (yellow dashed line in sagittal and transverse slices). (A,B) temperature and thermal dose vs. distance from the bone along the centre of HIFU beam. (C) Temperature and thermal dose profiles in the cross-section of the HIFU beam that intersects the near field MRI slice location (white oval in the image indicates the intersection).

large masses of soft tissue deep in the lower abdomen [13]. In contrast to uterine fibroids, OO are small bone lesions that are most commonly found in extremities and at variable depths from the skin. These differences often necessitate centring patients at one of the ends of the MR-HIFU table and using a custom table extension (Figure 2(A,B)). The need for such extensions has not been directly addressed by other groups that have performed MR-HIFU ablations in extremities, and our experience indicates that manufacturers should expand the variety of available shapes and sizes of table extensions to accommodate extremity treatments. Rotation and bending of the extremity that was required to centre the lesion in the middle of the treatment window may not always be feasible. These difficulties may be addressed with a transducer that can be positioned manually over the target

region [14]. The use of these new systems for extremity sonications is currently under investigation.

Design of MR-HIFU: acoustic coupling and skin protection

Possibility of skin and other off-target tissue burns is a potential risk during MR-HIFU ablation. Skin burns may arise from inadequate acoustic coupling leading to air bubbles in the acoustic beam path as well as off-target heating in tissues adjacent to skin. Acoustic coupling to the skin was achieved using a combination of liquid and solid ultrasound gel (Figure 2(E,F)). Air bubbles in the skin-gel interface were easily visible using an MRI sequence optimised for this purpose (Table 1). The risk of heat accumulation in off-target tissues is largely avoided by using "cooling periods" after each
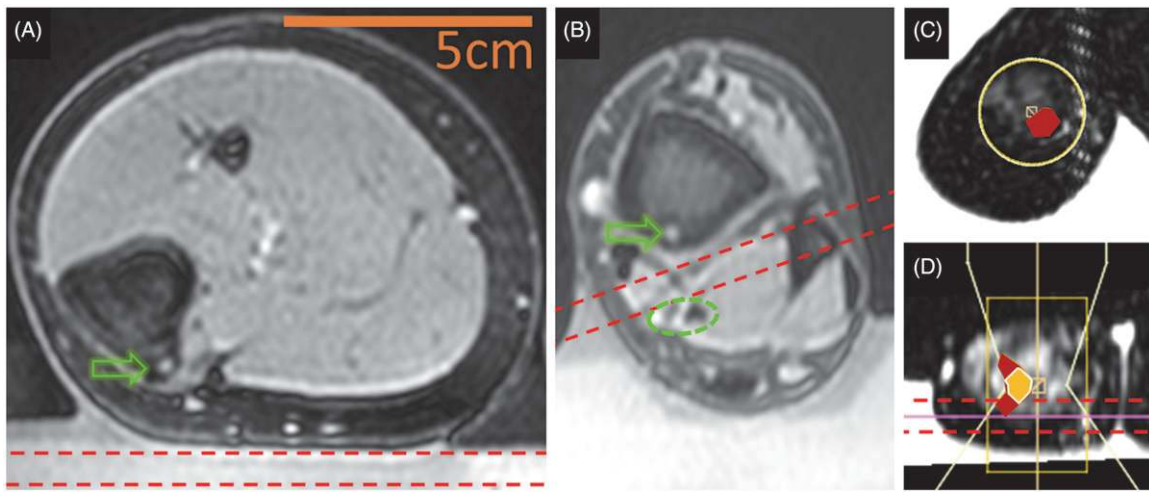
Figure 6. Estimation of near field heating and ensuring treatment safety. Bounds of an imaging slice (7 mm thick) dedicated to near field temperature monitoring are depicted using dashed lines. Green arrows indicate the location of OO nidus and a green dashed oval marks a neurovascular bundle that must be spared from ablation. (A) Positioning a slice dedicated to near field temperature monitoring may not be possible in the muscle and skin temperature may be approximated at the gel-skin interface (OO in tibia, Patient 7). (B) Near field monitoring slice may be placed between the targeted bone surface and a critical structure to ensure its safety (tibia, Patient 8). (C) Near field image through muscle and fat in the OO vicinity (phalanx, Patient 4). (D) Orthogonal T1-weighted images show that monitoring of near-field temperature in the phalanx. The HIFU beam is outlined along with areas of sub-lethal thermal effect (filled in red in C and D) and lethal thermal effect (white borders and yellow fill in D).

sonication that allow skin and other intervening tissues to cool. However, this safety measure noticeably impacts treatment time. Including the 3-min cooling periods between each sonication, the total sonication time per patient was 48 ± 15 min – more than 14 times greater than the time required for the actual sonications. Napoli et al. also reported that "effective treatment time" was several times shorter than "total length of treatment" [8]. Reducing or eliminating cooling periods between sonications could potentially cut treatment duration by as much as an order of magnitude, which is especially relevant in younger patients, all of whom require anaesthesia and sedation. This could be achieved by applying an initially acquired baseline scan to all sonications and ensuring adequate correction for magnetic drift, as recent work demonstrates [15]. For example, an early implementation of some of these changes allowed for treatment of large uterine fibroids [16].

The concern over skin heating is exacerbated by a lack of reliable real-time skin temperature measurement that would adequately capture the entire area at risk of off-target ablation. At best, MRI provides only a qualitative measurement of skin temperature, which cannot be obtained in real time [17]. Patients undergoing OO ablation must remain sedated during the procedure, and, therefore, the risk of skin damage may be greater during OO ablation than with uterine fibroid ablation, where the patients were awake during all procedures and could respond to pain. Our experience thus far suggests that real-time MRI thermometry both in muscle and in the gel adjacent to the skin provided useful information on skin temperature. In absence of a robust real-time skin temperature measurement, and lacking feedback from sedated patients, we employed both direct cooling of the skin (gel pads were cooled to 4 °C prior to the procedure) and standard cooling periods of 3 min to minimise the possibility of skin damage. Altogether, these precautions were

effective, and no skin burns were detected in our clinical trial, even in cases of lesions located close to 1 cm from the skin.

Treatment workflow: utility of awake pre-positioning

Since MR-HIFU ablation required anaesthesia/sedation in all younger patients, strategies that reduce or limit total procedure duration are important. In this regard, positioning and scanning patients on the MR-HIFU table prior to induction of anaesthesia/sedation was helpful for several reasons: (1) it allowed us to elicit patient feedback regarding areas of focal pressure and discomfort while the limb was positioned for treatment and decreased the likelihood of post-procedure pain and bruising due to inadequate padding on the MR-HIFU table, (2) it allowed us to ensure that selected MRI sequences optimally demonstrated the lesion and that it could be centred within the allowable treatment volume and (3) it allowed us to confirm that the limb positioning required for coupling and lesion accessibility to the HIFU beam path was achievable. This cannot always be accurately predicted from diagnostic images which are obtained in standard axial, sagittal and coronal anatomic planes rather than the position required for treatment. Thus, pre-positioning affords time for evaluation, discussion and adjustment of patient position by the HIFU treatment team and prevents unnecessary anaesthesia/sedation exposure. Similar pre-positioning steps were also used by other research groups in ablation of metastatic bone lesions with MR-HIFU [18].

Balance between soft tissue and bone damage

Heating within the bone occurs in large part via heat conduction from the cortex surface at the frequencies used in current clinical MR-HIFU devices (1.2 MHz herein). Practically, this means that the treatable depth beyond the surface of the bone cortex is limited by the extent of acceptable

ablation of soft tissues adjacent to the bone. Our data demonstrate that the extent of ablation is significantly greater in the bone than in soft tissue (Table 3). If this preferential targeting of bone continues to hold true in subsequent treatments, its generalisation may allow treatment closer to the skin and neurovascular tissues and deeper in the bone. Use of computer simulations that incorporate tissue attenuation and geometry of prospective patients has the potential to further reduce overall treatment time and improve the safety of the procedure by providing the clinical team with initial sonication parameter values.

Generalisation of MR-HIFU ablation of OO across available treatment platforms

Comparison to recent work reveals that these treatments may be generalisable across device manufacturers. The lesions treated herein were at a depth of 3.2 ± 1.6 cm relative to the skin and appear similar to those treated in a recent trial of an older patient cohort by Geiger et al. and Napoli et al. [8,9]. While they used an MR-HIFU by a different manufacturer, the sonication methodology relied on similar sonication durations ($\sim$22 s vs. 18 ± 5 s we used). Average sonication energy was also similar to our trial, albeit slightly greater (1180 ± 736 J compared to our 968 ± 700 J). Our approach included the use of a greater number of sonications overall, however (11 ± 4), whereas Geiger et al. used only 7 ± 3 sonications. Growing experience allowed sonication power to be increased more rapidly following initial test sonications, thus allowing us to decrease the overall number of sonications, reducing treatment duration in subsequent patients (Figure 3).

Effect of target location, size and composition: contrast to other lesions treated with MR-HIFU

Due to the differences in lesion size and composition, ablation of OO is not easy to relate to earlier clinical trials of metastatic bone cancer or soft tissue lesions, such as uterine fibroids. OO lesions are much smaller than the malignant tumours reported to have been treated with MR-HIFU (median and range were 0.82 (0.4–2.4) cm^3 herein compared to a median and range of 75.4 (0.4–1341) cm^3 in metastatic disease [19] and several hundred cm^3 for uterine fibroids [20]). While the depth of bony metastases treated with MR-HIFU is not readily available, they are deeper than the typical OO lesions we have treated [19]. The lesions, we report on are also more shallow compared to the deeper sonications performed in uterine fibroids (6.8 ± 0.5 cm [20]). Many of the sonication parameters and approaches differ among these applications, and thus far, published reports show that large and deep soft tissue targets, such as uterine fibroids are best treated with high-energy sonications at around 1 MHz [20]. In the case of bone targets, sonication power may be lower due to the several fold greater attenuation of ultrasound by cortical bone in the therapeutic frequency range [21]. Larger bony lesions require more sonications at more distinct locations [18,22], which requires longer sonication times than the smaller OO lesions described herein. In contrast, OO may be targeted with only a few high-energy sonications that cover the OO nidus and adjacent periosteum, with little risk to intervening tissues.

Future directions

In addition to development of MR-HIFU systems specifically designed for bone ablation, several improvements to the current tabletop-integrated systems have the potential to impact treatment quality. Overall treatment quality may be further improved with availability of HIFU-compatible MRI coils specifically designed for extremity imaging, which could allow 3D MR thermometry in less vascularised regions, such as the OO nidus. Software-based prediction of target and near field tissue cooling rate, as well as elimination or reduction of post-sonication cooling periods can further reduce the total treatment time.

Conclusions

MR-HIFU ablation of OO in children and young adults was technically feasible, without any serious treatment-attributable adverse events in eight patients. There was a learning curve in all aspects of this procedure, ranging from patient positioning to selection of optimal sonication parameters to reduction of procedure duration. The data reported here provide technical guidance to teams and centres that are performing these novel treatments, potentially improving patient selection as well as treatment workflow and quality. There are opportunities to improve design of MR-HIFU hardware and software to optimise OO treatment. Such improvements may allow for treatment of lesions located deeper within bone as well as to improve real-time imaging feedback showing the extent of ablation during the procedure.

References

[1] Atesok KI, Alman BA, Schemitsch EH, et al. (2011). Osteoid osteoma and osteoblastoma. J Am Acad Orthop Surg 19:678–89.

[2] Peterson JJ, Fenton DS, Czervionke LF, Education MFfM, Research. (2008). Image-guided Musculoskeletal Intervention. Philadelphia, PA: Saunders/Elsevier.

[3] Cantwell CP, Obyrne J, Eustace S. (2004). Current trends in treatment of osteoid osteoma with an emphasis on radiofrequency ablation. Eur Radiol 14:607–17.

[4] Rosenthal DI, Hornicek FJ, Torriani M, et al. (2003). Osteoid osteoma: percutaneous treatment with radiofrequency energy. Radiology 229:171–5.

[5] Bruners P, Penzkofer T, Gunther RW, Mahnken A. (2009). [Percutaneous radiofrequency ablation of osteoid osteomas: technique and results]. Rofo181:740–7.

[6] Hsiao YH, Kuo SJ, Tsai HD, et al. (2016). Clinical application of high-intensity focused ultrasound in cancer therapy. J Cancer 7:225–31.

[7] Liberman B, Gianfelice D, Inbar Y, et al. (2009). Pain palliation in patients with bone metastases using MR-guided focused ultrasound surgery: a multicenter study. Ann Surg Oncol 16:140–6.

[8] Napoli A, Mastantuono M, Cavallo Marincola B, et al. (2013). Osteoid osteoma: MR-guided focused ultrasound for entirely noninvasive treatment. Radiology 267:514–21.

[9] Geiger D, Napoli A, Conchiglia A, et al. (2014). MR-guided focused ultrasound (MRgFUS) ablation for the treatment of nonspinal osteoid osteoma: a prospective multicenter evaluation. J Bone Joint Surg Am 96:743–51.

[10] Safety and Feasibility of MR-Guided High Intensity Focused Ultrasound (MR-HIFU) Ablation of Osteoid Osteoma in Children. (2016). Children's Research Institute U.S. National Institutes of Health. Available from: https://clinicaltrials.gov/ct2/show/NCT02349971.

[11] Ishihara Y, Calderon A, Watanabe H, et al. (1995). A precise and fast temperature mapping using water proton chemical shift. Magn Reson Med 34:814–23.

[12] Yarmolenko PS, Moon EJ, Landon C, et al. (2011). Thresholds for thermal damage to normal tissues: an update. Int J Hyperthermia 27:320–43.

[13] Pron G. (2015). Magnetic resonance-guided high-intensity focused ultrasound (MRgHIFU) treatment of symptomatic uterine fibroids: an evidence-based analysis. Ont Health Technol Assess Ser 15:1–86.

[14] Joo B, Park MS, Lee SH, et al. (2015). Pain palliation in patients with bone metastases using magnetic resonance-guided focused ultrasound with conformal bone system: a preliminary report. Yonsei Med J 56:503–9.

[15] Bitton RR, Webb TD, Pauly KB, Ghanouni P. (2016). Improving thermal dose accuracy in magnetic resonance-guided focused ultrasound surgery: long-term thermometry using a prior baseline as a reference. J Magn Reson Imaging 43:181–9.

[16] Park MJ, Kim YS, Keserci B, et al. (2013). Volumetric MR-guided high-intensity focused ultrasound ablation of uterine fibroids: treatment speed and factors influencing speed. Eur Radiol 23:943–50.

[17] Rieke V, Butts Pauly K. (2008). MR thermometry. J Magn Reson Imaging 27:376–90.

[18] Napoli A, Anzidei M, Marincola BC, et al. (2013). MR imaging-guided focused ultrasound for treatment of bone metastasis. Radiographics 33:1555–68.

[19] Hurwitz MD, Ghanouni P, Kanaev SV, et al. (2014). Magnetic resonance-guided focused ultrasound for patients with painful bone metastases: phase III trial results. J Natl Cancer Inst106:dju082.

[20] Kim YS, Keserci B, Partanen A, et al. (2012). Volumetric MR-HIFU ablation of uterine fibroids: role of treatment cell size in the improvement of energy efficiency. Eur J Radiol 81:3652–9.

[21] Duck FA. (1990). Physical properties of tissue: a comprehensive reference book. London: Academic Press.

[22] Huisman M, Lam MK, Bartels LW, et al. (2014). Feasibility of volumetric MRI-guided high intensity focused ultrasound (MR-HIFU) for painful bone metastases. J Ther Ultrasound 2:16.